Ring-like shaped charge modulations in the *t-J* model with long-range Coulomb interaction

Matías Bejas [1], Roland Zeyher,[2] and Andrés Greco [1,2]

[1]*Facultad de Ciencias Exactas, Ingeniería, y Agrimensura and Instituto de Física Rosario (UNR-CONICET),*
Avenida Pellegrini 250, 2000 Rosario, Argentina
[2]*Max-Planck-Institut für Festkörperforschung, Heisenbergstraße 1, D-70569 Stuttgart, Germany*

The study of the charge excitations in cuprates is presently an interesting topic because of the development of new and precise x-ray experiments. Based on a large-N formulation of the two-dimensional t-J model, which allows us to consider all possible charge excitations on an equal footing, we investigate the charge spectrum for both electron- and hole-doped cases. In both cases, the instability toward phase separation, which has momentum modulation $\mathbf{q} = (0, 0)$, is found to be robust in a large region of the doping-temperature phase diagram. If a short-range Coulomb repulsion is included the phase separation region shrinks, but the instability remains at $\mathbf{q} = (0, 0)$. If on the other hand a two-dimensional long-range Coulomb interaction is included the instability sets in at $\mathbf{q}$ momenta forming a ring around $\mathbf{q} = (0, 0)$. The computed charge spectrum in the translation-invariant phase shows well-formed rings. We discuss our results in the light of recent x-ray experiments in electron- and hole-doped cuprates, where ring-like shaped charge modulations have been reported.

I. INTRODUCTION

Recent progress in x-ray scattering techniques revealed the presence of a charge order (CO), with CO momentum along the axial direction $[(0, 0)$-$(\pi, 0)]$, in hole-doped cuprates (h-cuprates) [1–11] as well as in electron-doped cuprates (e-cuprates) [12–14]. The CO tendency in h- and e-cuprates was intensively studied theoretically [15,15–30], but its origin is still under debate. This topic is of large interest because it reveals the importance of charge fluctuations even in the deep underdoped region, were magnetic fluctuations are usually considered to be the dominant excitations.

Another interesting topic of the CO is its internal symmetry. For a long time it was generally believed that d-wave symmetry is realized [7]. However, recently it was found that the CO has a predominant s-wave symmetry [31]. More recently, it also was found that the CO extends along all directions in the same manner through the Brillouin zone (BZ), forming a ring. Such a ring had been observed in resonant x-ray scattering in the h-cuprate $Bi_2Sr_2CaCu_2O_{8+\delta}$ [32]. A similar ring has also been reported in e-cuprates [33].

In the following we present a theory for ring formation based on the t-J model treated in the large-N approximation. The large-N approximation, where the spin index is extended from two projections to N and the small parameter $1/N$ is taken for controlling the approximation, was extensively studied in Refs. [34–43], to name a few. This approximation has the disadvantage that spin fluctuations are suppressed; i.e., the Mott insulator is not captured properly. However, all possible charge fluctuations can be treated on an equal footing making the method of potential interest for studying the charge excitations detected in the new x-ray scattering experiments. Based on the t-J model on a square lattice and in the presence

of a long-range Coulomb interaction (t-J-V model) we will show that ring-like shaped charge density waves (CDWs) are expected from the local charge susceptibility. We will discuss similarities and differences with the experiments, for both, e- and h-cuprates.

In Sec. II we will show a summary of the theoretical method, Sec. III contains our results, Sec. IV a comparison with experiment, and Sec. V the conclusion.

II. MATHEMATICAL FRAMEWORK

We study the t-J model on a square lattice including the two-dimensional long-range Coulomb interaction. The Hamiltonian is given by

$$H = - \sum_{i,j,\sigma} t_{ij} \tilde{c}_{i\sigma}^{\dagger} \tilde{c}_{j\sigma} + J \sum_{\langle i,j \rangle} \left(\vec{S}_i \cdot \vec{S}_j - \frac{1}{4} n_i n_j \right)$$
$$+ \frac{1}{2} \sum_{i,j} V_{ij} n_i n_j, \tag{1}$$

where $\tilde{c}_{i\sigma}^{\dagger}$ ($\tilde{c}_{i\sigma}$) are creation (annihilation) operators for electrons with spin σ ($=\uparrow, \downarrow$) in the Fock space without double occupancy at any site, $n_i = \sum_{\sigma} \tilde{c}_{i\sigma}^{\dagger} \tilde{c}_{i\sigma}$ is the electron density operator, $\vec{S}_i$ is the spin operator, and the sites i and j run over a two-dimensional square lattice. The hopping t_{ij} takes the value t (t') between the first (second) nearest-neighbor sites on the square lattice. $\langle i, j \rangle$ denotes the nearest-neighbor sites and J is the exchange interaction. V_{ij} is the long-range Coulomb interaction on the two-dimensional lattice.

In this paper we will follow the large-N formulation of Ref. [37]. In the large-N limit the t-J model becomes equivalent to the following effective Hamiltonian in terms of usual

creation and annihilation operators,

$$H_{\text{eff}} = \sum_{\mathbf{k}\sigma} \epsilon(\mathbf{k}) c_\sigma^\dagger(\mathbf{k}) c_\sigma(\mathbf{k}) - \frac{N_s}{2} \sum_{\alpha=1}^{6} \sum_{\mathbf{q}} \rho_\alpha'(\mathbf{q}) \rho_\alpha^\dagger(\mathbf{q}). \quad (2)$$

At leading order, the electron dispersion $\epsilon(\mathbf{k})$ is obtained as

$$\epsilon(\mathbf{k}) = -2\left(t\frac{\delta}{2} + \Delta\right)(\cos k_x + \cos k_y) - 4t'\frac{\delta}{2}\cos k_x \cos k_y - \mu. \quad (3)$$

While the dispersion is similar to the noninteracting case, the hopping integrals t and t' are renormalized by a factor $\delta/2$ where δ is the doping rate. The quantity Δ in Eq. (3) is given by

$$\Delta = \frac{J}{4N_s} \sum_{\mathbf{k}} (\cos k_x + \cos k_y) n_F(\epsilon(\mathbf{k})), \quad (4)$$

where n_F is the Fermi function, and N_s the total number of lattice sites. For a given doping δ, the chemical potential μ and Δ are determined self-consistently by solving Eq. (4) and

$$(1-\delta) = \frac{2}{N_s} \sum_{\mathbf{k}} n_F(\epsilon(\mathbf{k})). \quad (5)$$

The second term in Eq. (2) represents an effective interaction, where

$$\rho_\alpha'(\mathbf{q}) = \frac{1}{N_s} \sum_{\mathbf{k}\sigma} E_\alpha(\mathbf{k}, \mathbf{q}) c_\sigma^\dagger(\mathbf{k}+\mathbf{q}) c_\sigma(\mathbf{k}), \quad (6)$$

$$\rho_\beta(\mathbf{q}) = \frac{1}{N_s} \sum_{\mathbf{k}\sigma} F_\beta(\mathbf{k}) c_\sigma^\dagger(\mathbf{k}+\mathbf{q}) c_\sigma(\mathbf{k}), \quad (7)$$

with

$$E_\alpha(\mathbf{k}, \mathbf{q})$$
$$= [1, t(\mathbf{k}+\mathbf{q}) + J(\mathbf{q}) - V(\mathbf{q}), \gamma_3(\mathbf{k}), \gamma_4(\mathbf{k}), \gamma_5(\mathbf{k}), \gamma_6(\mathbf{k})] \quad (8)$$

and

$$F_\beta(\mathbf{k}) = [t(\mathbf{k}), 1, 2J\gamma_3(\mathbf{k}), 2J\gamma_4(\mathbf{k}), 2J\gamma_5(\mathbf{k}), 2J\gamma_6(\mathbf{k})], \quad (9)$$

where $t(\mathbf{k}) = -2t(\cos k_x + \cos k_y) - 4t'\cos k_x \cos k_y$ and $J(\mathbf{q}) = J(\cos q_x + \cos q_y)$ are the hopping and the magnetic exchange in the momentum space. $V(\mathbf{q})$ is the expression for the two-dimensional long-range Coulomb interaction in the momentum space. In Ref. [42] the long-range Coulomb interaction V_{ij} in a square plane embedded in a three-dimensional lattice is written in momentum space as

$$V(\mathbf{q}) = \frac{V_c}{\sqrt{A^2(\mathbf{q}) - 1}}, \quad (10)$$

where $A(\mathbf{q}) = \alpha(2 - \cos q_x - \cos q_y) + 1$. In Eq. (10) $V_c = e^2 c(2\epsilon_\perp a^2)^{-1}$ and $\alpha = \tilde{\epsilon}(a/c)^{-2}$, with $\tilde{\epsilon} = \epsilon_\parallel/\epsilon_\perp$, where $\epsilon_\parallel$ and $\epsilon_\perp$ are the dielectric constants parallel and perpendicular

to the planes, respectively, a is the lattice constant in the plane, and c the distance between them. The electric charge of electrons is denoted as e.

In addition,

$$\gamma_{3,5} = (\cos k_x \pm \cos k_y)/2, \quad \gamma_{4,6} = (\sin k_x \pm \sin k_y)/2, \quad (11)$$

where the subscripts 3 and 4 refer to the +, and 5 and 6 to the − sign.

Using Eqs. (6) and (7) one easily verifies that the sum of the terms $\alpha = 3$–6 represents the Heisenberg exchange interaction. The terms $\alpha = 1, 2$ originate from the constraint which acts in H_{eff} as a two-particle interaction. H_{eff} represents the original t-J model in the large-N limit.

In this framework, all charge susceptibilities are treated on equal footing and can be calculated as

$$\chi_{\alpha\beta}(q) = \sum_\gamma \chi_{\alpha\gamma}^{(0)}(q)[1 + \chi^{(0)}(q)]_{\gamma\beta}^{-1}. \quad (12)$$

Here we used the abbreviation $q = (i\omega_n, \mathbf{q})$ with the bosonic Matsubara frequencies $\omega_n = 2\pi T n$, where T is the temperature. $\chi^{(0)}(q)$ stands for a single bubble and is given analytically by the expression

$$\chi_{\alpha\beta}^{(0)}(\mathbf{q}, i\omega_n)$$
$$= \frac{1}{N_s} \sum_{\mathbf{k}} E_\alpha(\mathbf{k}, \mathbf{q}) F_\beta(\mathbf{k}) \frac{n_F(\epsilon(\mathbf{k}+\mathbf{q})) - n_F(\epsilon(\mathbf{k}))}{\epsilon(\mathbf{k}+\mathbf{q}) - \epsilon(\mathbf{k}) - i\omega_n}. \quad (13)$$

In Eq. (12) there are two types of charge fluctuations: on-site (s-wave) usual charge-charge correlation function, which is contained in the channels 1,2, and bond-charge fluctuations triggered by J with internal symmetry s and d, included the flux phase [15,44], that belong to the channels 3 to 6. It was demonstrated in Ref. [45] that there is a dual structure in energy, and the channels 3 to 6 are practically decoupled from the channels 1,2. As discussed in Ref. [37], the usual charge-charge correlation function is $\chi_{\text{ch}}(\mathbf{q}, \omega) = \chi_{12}(\mathbf{q}, \omega)$ in Eq. (12). Here, we will mainly focus on $\chi_{12}(\mathbf{q}, \omega)$, since the bond-charge fluctuations play a minor role in the present study.

In the following we will consider V_c and α in $V(\mathbf{q})$ as independent parameters. t is considered the unit of energy, and a the length unit. For a clear presentation of the ring structures we chose $\alpha = 1$ and $V_c = 1$, while in Sec. IV we use realistic values of V_c and α in order to make contact with experiments.

It is important to note that although Eq. (12) looks like a usual RPA form, this expression is obtained in a large-N approximation [37]. For instance, the single bubble matrix [Eq. (13)] contains the form factors E_α and F_β which are derived from the t-J model in the large-N approximation. Some results in present paper were also obtained with the equivalent formulation of Ref. [15].

III. RESULTS

A. Results for h-cuprates

For h-cuprates we chose $J = 0.3$ and $t' = -0.3$. In Fig. 1 we present the phase diagram in the doping δ and temperature
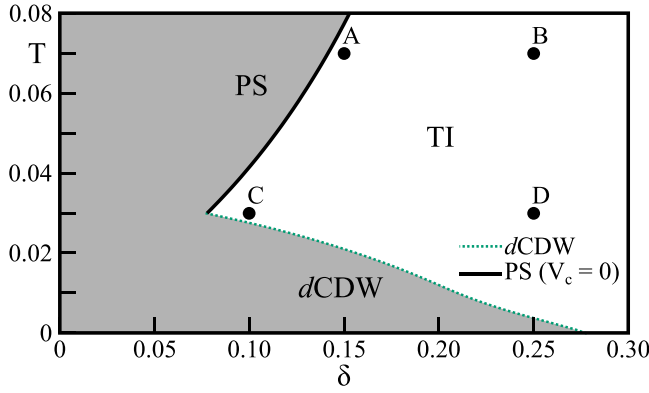
FIG. 1. Phase diagram in the δ-T plane without Coulomb interaction, i.e., $V_c = 0$. Solid (dotted) line is the onset of the phase separation (dCDW) instability. A, B, C, and D are four selected points in the translation-invariant phase (TI) which will be analyzed in Fig. 2.

FIG. 3. Phase diagram in the δ-T plane with long-range Coulomb interaction. Solid (dotted) line is the onset of the ring phase (dCDW) instability. A, B, C, and D are four selected points in the translation-invariant phase which will be analyzed in Fig. 4.

T plane for $V_c = 0$, i.e., no long-range Coulomb interaction is present. The dotted line marks the onset of the flux phase instability [15,44]. The flux phase is equivalent to the d-wave charge density wave (dCDW) introduced phenomenologically in Ref. [46]. The solid line represents the onset for the instability toward phase separation (PS) [15]. That is, for dopings and temperatures along the solid line the real part of the charge-charge susceptibility $\mathrm{Re}\,\chi_{ch}(\mathbf{q}=0,\omega=0)$ diverges. The four points A, B, C, and D in Fig. 1 will be discussed below. They are located in the translation-invariant phase where our large-N Fermi liquid phase is stable. In the gray region the translation-invariant phase is unstable. Our calculations are performed always in the translation-invariant phase.

In Fig. 2(a) we show $\mathrm{Re}\,\chi_{ch}(\mathbf{q},\omega=0)$ for $\mathbf{q}$ along the path (π,π)-$(0,0)$-$(\pi,0)$-(π,π) for the points A–D in Fig. 1. Since A and C are close to the PS instability line, $\mathrm{Re}\,\chi_{ch}(\mathbf{q},\omega=0)$ shows sharp and large peaks located at $\mathbf{q}=(0,0)$. If both A and C move to lower dopings and touch the solid line they will show a δ function at $\mathbf{q}=(0,0)$ signaling the long-range order for PS. The points B and D also show peaks at $\mathbf{q}=(0,0)$, but they are broader and less intense than in A and C. That is because the points B and D are far from the PS line, and the fluctuations of the PS phase are weaker in B and D than in A and C. The point C is also close to the dCDW instability line; however, as discussed above, bond-charge and the usual
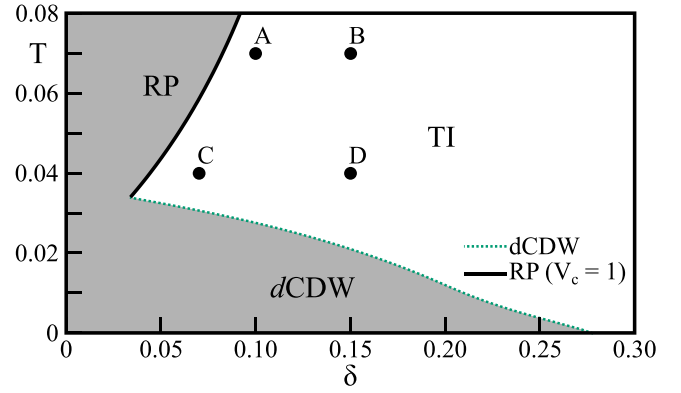
charge-charge correlations are decoupled. Then, the effect of dCDW on χ_{ch} is negligible. The peaks at $\mathbf{q}=(0,0)$ appear as disks in the color intensity maps for $\mathrm{Re}\,\chi_{ch}(\mathbf{q},\omega=0)$ over the full BZ depicted in Figs. 2(b)–2(e). For the points A and C, close to the PS instability line, the disks are small and intense while for B and D are broader and with much lower intensity.

The situation changes when we include the long-range Coulomb repulsion. In Fig. 3 we show the phase diagram including the long-range Coulomb interaction $V(\mathbf{q})$. Note that the dCDW is not affected by the presence of the long-range Coulomb interaction, showing the decoupling between channels 3–6 and the channels 1,2 as discussed above. The solid line is clearly shifted to lower dopings showing a larger region in the phase diagram where the translation-invariant phase is stable. However, the nature of the charge instability at the solid line line is no longer PS. In Fig. 4(a) we show the $\mathrm{Re}\,\chi_{ch}(\mathbf{q},\omega=0)$ for $\mathbf{q}$ along the path (π,π)-$(0,0)$-$(\pi,0)$-(π,π) for the points located at A–D in Fig. 3. Now, in the presence of the long-range Coulomb interaction, the peaks are not located at $\mathbf{q}=(0,0)$ but instead they are shifted from $(0,0)$. As in the case of Fig. 2, the peaks are more intense and sharper for A and C than for B and D. Figures 4(b)–4(e) show color intensity maps for $\mathrm{Re}\,\chi_{ch}(\mathbf{q},\omega=0)$ on the BZ for the selected points A, B, C, and D on the

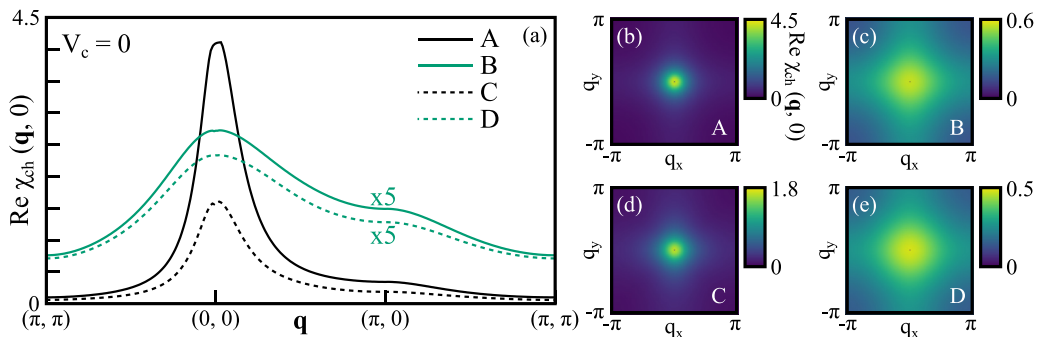FIG. 2. (a) $\mathrm{Re}\,\chi_{ch}(\mathbf{q},\omega=0)$ for $\mathbf{q}$ along the path (π,π)-$(0,0)$-$(\pi,0)$-(π,π) for the selected points A, B, C, and D in Fig. 1. Note that the intensity at B and D is multiplied by 5. (b)–(e) Color intensity maps on the Brillouin zone of $\mathrm{Re}\,\chi_{ch}(\mathbf{q},\omega=0)$ for the points A, B, C, and D, respectively.

FIG. 4. $\mathrm{Re}\chi_{ch}(\mathbf{q}, \omega = 0)$ for $\mathbf{q}$ along the path (π, π)-$(0, 0)$-$(\pi, 0)$-(π, π) for the selected points A, B, C, and D in Fig. 3. (b)–(e) Color intensity maps on the Brillouin zone of $\mathrm{Re}\chi_{ch}(\mathbf{q}, \omega = 0)$ for the points A, B, C, and D, respectively.
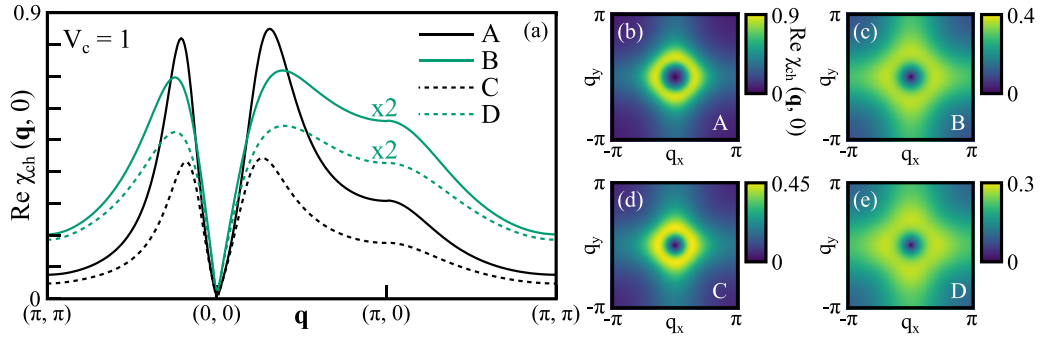
phase diagram, respectively. Interestingly, the intensity maps show clear and well-defined ring-shaped charge modulations around $\mathbf{q} = (0, 0)$. For this reason we have called the phase that occurs at the onset of the solid line the ring phase (RP). Note that, as they are farther from the instability line, the rings for B and D are less intense and more diffused than for A and C.

B. Results for e-cuprates

The t-J model is defined in the space where the presence of two electrons per site is prohibited. In order to present calculations for e-cuprates we proceed as usual: we make a particle-hole transformation which requires a sign change for t' [47–50]. Here we chose $J = 0.3$ and $t' = 0.3$.

Figure 5(a) shows the phase diagram for $V_c = 0$. Comparing Fig. 1 and Fig. 5(a) we can see that there is a larger tendency for PS in the electron-doped case [50]. Figure 5(b) is equivalent to Fig. 2 for the h-cuprates, and show that for $V_c = 0$ the local charge instability is toward the usual PS with ordered momentum $\mathbf{q} = 0$. Then, the momentum map shows

disks [Figs. 5(c)–5(f)] instead of rings. Similar to Fig. 3 and Fig. 4, Fig. 6 shows that rings are formed in the translation-invariant phase near the RP instability when the long-range Coulomb is included. That is, ring-shaped charge modulations also occurs in e-cuprates. Since now the region for the translation-invariant phase is much more extended in Fig. 6(a) than in Fig. 5(a), we also show the leading instabilities from the channels 3–6, triggered by J. The flux phase is the leading phase in the temperature range 0.01–0.03 and $\delta < 0.10$. For larger doping and lower temperatures a bond-order phase (BOP$_{x\bar{y}}$) is the leading instability [50].

IV. COMPARISON WITH EXPERIMENTS

Resonant x-ray scattering on $\mathrm{Bi_2Sr_2CaCu_2O_{8+\delta}}$ discovered a dynamic quasicircular charge pattern [32], i.e, ring-like shaped charge modulations. The authors of Ref. [32] proposed an explanation for the rings. Assuming the random phase approximation (RPA) [51] and a Coulomb repulsion of the form $V(\mathbf{q}) = V_c(\mathbf{q}) + U(\mathbf{q})$, where $V_c(\mathbf{q})$ is a two-dimensional long-range Coulomb interaction and $U(\mathbf{q})$ is a
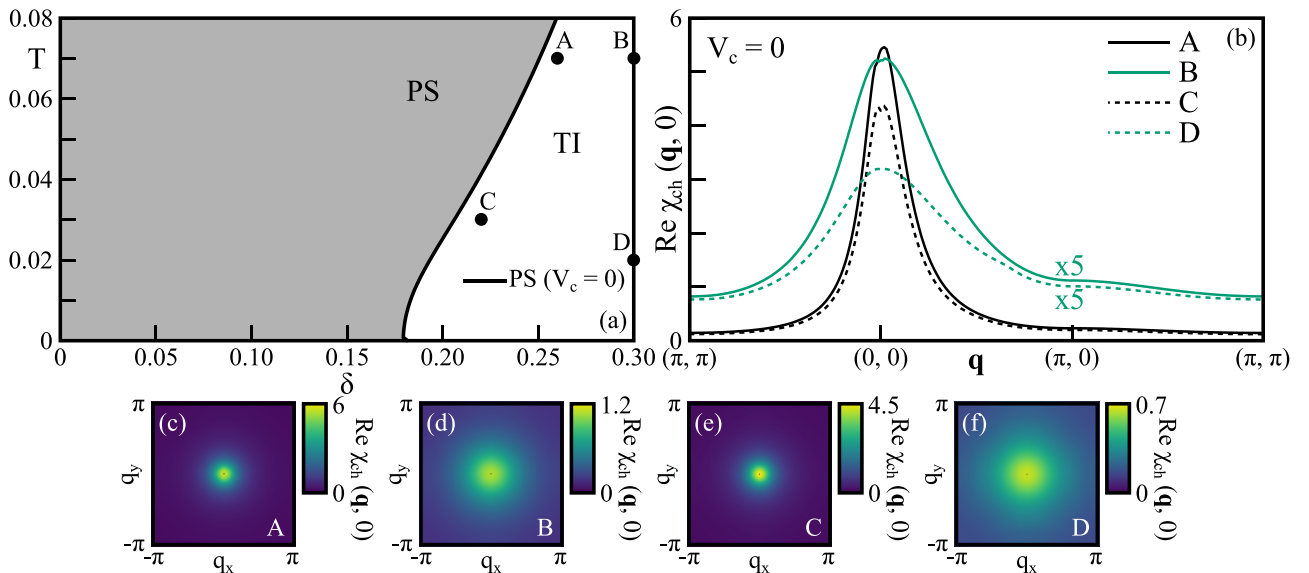

FIG. 5. (a) Phase diagram for e-cuprates without Coulomb interaction. Momentum cuts (b), and maps (c)–(f) of $\mathrm{Re}\chi_{ch}(\mathbf{q}, \omega = 0)$ for the selected points A–D.
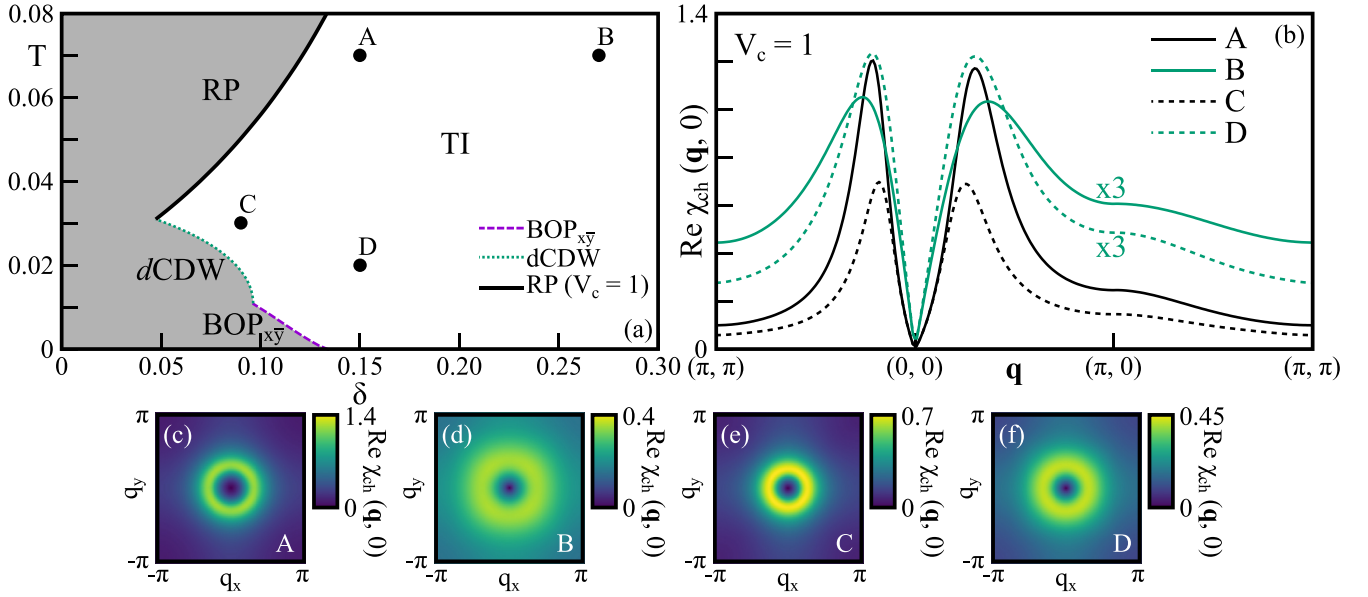
FIG. 6. (a) Phase diagram for e-cuprates with long-range Coulomb interaction. In the presence of a long-range Coulomb interaction the homogeneous translation-invariant phase extends and dCDW (dotted line) and BOP$_{x\bar{y}}$ instabilities occur. Momentum cuts (b), and maps (c)–(f) of Re$\chi_{ch}(\mathbf{q}, \omega = 0)$ for the selected points A–D.

short-range Coulomb potential, the charge-charge correlation function was calculated. Although both $V_c(\mathbf{q})$ and $U(\mathbf{q})$ have a monotonic behavior, the sum of both show a nonmonotonic behavior with a minimum at a given $\mathbf{q}$ that determines the quasicircular pattern. Besides the proposed RPA does not describe the observed rings in detail, RPA works for weakly correlated systems but cuprates are considered strongly correlated. In this paper we have studied the t-J model, which is a model more appropriated for cuprates [52]. The t-J model contains the competition between kinetic energy and PS [47,48,50,53], which is characterized by a strong peak at $\mathbf{q} = (0, 0)$ in the usual charge-charge correlation function. This competition originates in the constraint that prohibits double occupancy, and it is missing in RPA. It is well known that the inclusion of a short-range Coulomb repulsion reduces the PS region in the doping and temperature phase diagram [50]. However, if instead of including a short-range we applied a long-range Coulomb interaction, we found rings as shown in the previous sections. Interestingly the radii of the rings are of the order of 0.3π–0.4π, which is close to the radius reported in the experiment [32,33]; see for instance Figs. 4(b)–4(e).

In previous sections, for a clearer presentation of the results we have chosen the parameter values $\alpha = 1$ and $V_c = 1$ in the long-range Coulomb potential. What happens if we use more suitable parameters as those used for describing the recently observed low-energy plasmons in resonant inelastic x-ray scattering (RIXS) [54–56]? In Fig. 7 we present results for h-cuprates ($t' = -0.3$), and we chose $\alpha = 4$ and $V_c = 20$ which are of the order of those used in Refs. [54–56] in the context of the t-J-V model. The instability line toward the ring phase is much more shrunken.

In Figs. 7(b)–7(d) we show color intensity maps for the three chosen points A, B, and C in panel (a). These intensity maps show that the largest intensity occurs along the axial direction as in the experiment [32]. Then, in contrast to the theoretical study presented in Ref. [32], our calcu-

lation captures the anisotropy behavior of the quasicircular charge pattern. In addition, as discussed in Ref. [32], our rings are dynamic, since they occur in the translation-invariant phase.

Up to now we have discussed the ring-shaped structures by analyzing Re$\chi_{ch}(\mathbf{q}, \omega = 0)$. In Ref. [32] the rings where discussed by using resonant x-ray scattering (RXS) and energy-integrated RIXS. RXS measures the equal-time
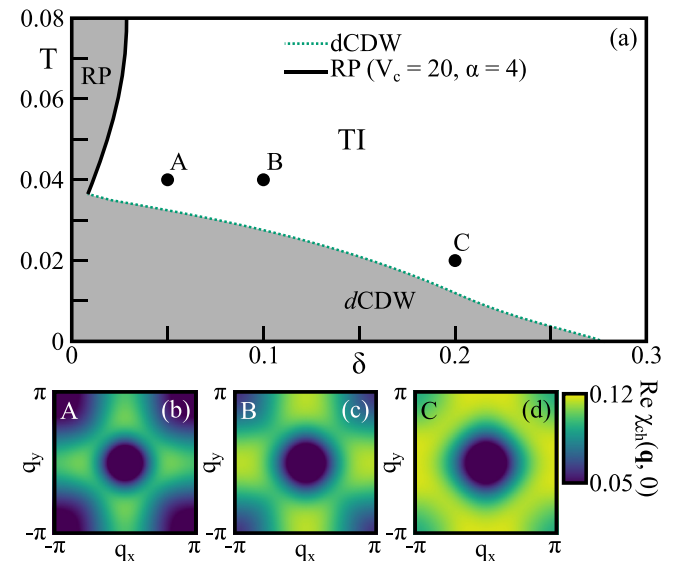

FIG. 7. (a) Phase diagram for h-cuprates for realistic long-range Coulomb parameters. (b)–(d) Color intensity map on the Brillouin zone for Re$\chi_{ch}(\mathbf{q}, \omega = 0)$ for the selected points A, B, and C, respectively.
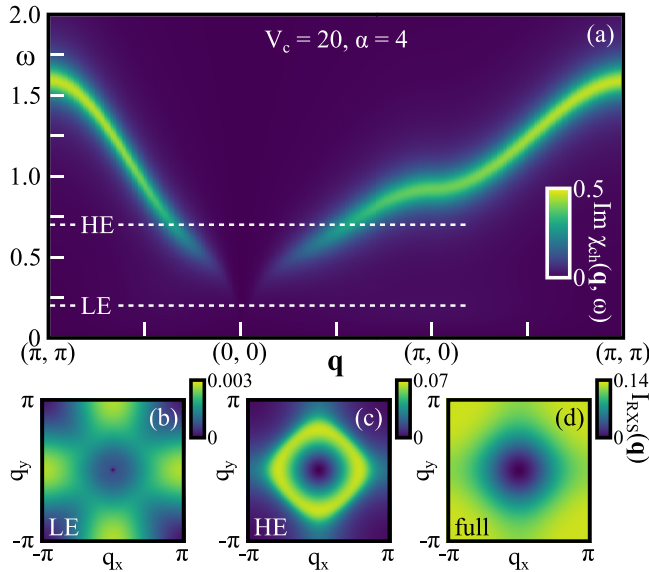
FIG. 8. (a) Momentum-energy map of $\mathrm{Im}\chi_{ch}(\mathbf{q}, \omega)$ along the path (π, π)-$(0,0)$-$(\pi, 0)$-(π, π) for the point B in Fig. 7(a). The horizontal dashed lines indicate the limits for the energy integration discussed in the text. (b) Color intensity map on the Brillouin zone of the low-energy (LE) integration of $\mathrm{Im}\chi_{ch}(\mathbf{q}, \omega)$. (c) The same as (b) for the high-energy (HE) integration. (d) The same as (b) and (c) for the full energy range, i.e., from $\omega = 0$ to infinity.

correlation function,

$$I_{RXS}(\mathbf{q}) = \int_{-\infty}^{\infty} \mathrm{Im}\chi_{ch}(\mathbf{q}, \omega)[n_B(\omega) + 1]d\omega$$
$$= \int_{0}^{\infty} \mathrm{Im}\chi_{ch}(\mathbf{q}, \omega)[2n_B(\omega) + 1]d\omega, \quad (14)$$

where $n_B(\omega)$ is the Bose factor, and $\mathrm{Im}\chi_{ch}(\mathbf{q}, \omega)$ is proportional to the RIXS spectrum.

In Fig. 8(a) we show the momentum-energy map of $\mathrm{Im}\chi_{ch}(\mathbf{q}, \omega)$ for the point B in Fig. 7(a) along the path (π, π)-$(0,0)$-$(\pi, 0)$-(π, π). We obtain a two-dimensional plasmon branch which has similarities to the low-energy plasmons observed in cuprates [55–59]. What happens if we integrate the spectra of $\mathrm{Im}\chi_{ch}(\mathbf{q}, \omega)$ [Eq. (14)] in different energy windows? Figure 8(b) shows the result for a low-energy (LE) integration up to the dashed line indicated with LE in Fig. 8(a). As in the experiment, Fig. 8(b) shows the largest intensity along the axial directions. The obtained map is similar to that of Fig. 7(c) for $\mathrm{Re}\chi_{ch}(\mathbf{q}, \omega = 0)$, since the low-energy integration in Eq. (14) leads to $I_{RXS}(\mathbf{q}) \sim \mathrm{Re}\chi_{ch}(\mathbf{q}, \omega = 0)$. If instead we integrate in a high-energy window, up to the dashed line indicated with HE in Fig. 8(a), we collect contributions from the V-shaped dispersion, and rings are formed [Fig. 8(c)]. However, the signals along the axial and nodal direction have similar intensity; the stronger intensity along the axial direction is lost. If we integrate the entire energy spectra the rings are washed out [Fig. 8(d)], due to the contribution from the top of the 2D plasmon dispersion.

Although our model does not capture quantitatively all the experimental aspects, as the doping and temperature behavior of the intensity and radius of the rings, we think that the

similarities between our results and those reported in Ref. [32] for $Bi_2Sr_2CaCu_2O_{8+\delta}$ are remarkable. In fact, we agree with the authors of Ref. [32] on the importance of the long-range Coulomb interaction for the formation of the rings. It would be desirable to make more x-ray experiments for different members of the cuprate family as a function of doping and temperature.

Finally, in Ref. [32] it is suggested that the momentum of the observed stronger intensity along the axial direction matches the wave vector of the discussed axial CO [1–11]. It is important to mention that most of the theoretical studies about the CO [15,15–26] suggest that the CO occurs due to bond-order charge excitations, and have an internal form factor different from the isotropic s wave. The rings appear in our calculation in the usual s-wave charge-charge correlation function, as also proposed in Ref. [32]. While bond-order charge fluctuations occur in our calculation in the sector 3–6, usual charge excitations occur in the 1–2 sector, and both channels are mainly decoupled [45]. This is an interesting topic which needs more discussion, because a bond-order charge fluctuation scenario is completely different from the usual s-wave charge fluctuation picture.

V. CONCLUSION

Phase separation is an instability at $\mathbf{q} = (0, 0)$ of the charge-charge correlation function. PS exists in the t-J-V model even for $J = V = 0$. Thus, only the first term in Eq. (1) is present. This means that the constraint which prohibits double occupancy plays a central role in the instability toward PS. It is well known that PS may cover a large region of the phase diagram, and the inclusion of a short-range Coulomb interaction reduces the PS region. This picture changes drastically if a long-range Coulomb interaction is included to cancel PS. In this case, although the instability region is reduced, the momenta $\mathbf{q}$ where the instability takes place is no longer $\mathbf{q} = (0, 0)$ and the ordered momenta follows a ring-like shape around $\mathbf{q} = (0, 0)$, leading to what we have called a ring phase. Interestingly, the charge excitation spectrum in the translation-invariant phase shows well-defined ring-shaped charge modulations, for both e-cuprates and h-cuprates. It is worth pointing out that although we compute the charge-charge correlation function at $\omega = 0$, this does not mean that the rings are static. As we are in the translation-invariant phase, the rings are formed by fluctuations in the proximity of the ring phase instability. The presence of rings is not difficult to understand. The long-range Coulomb interaction is strongly peaked at $\mathbf{q} = (0, 0)$ and decays with increasing $\mathbf{q}$. If the system shows PS, under the presence of the long-range Coulomb interaction the charge accumulation at $\mathbf{q} = (0, 0)$ is expelled, and rings are developed. Thus, the wave vector $\mathbf{Q}$, whose magnitude is associated with the radius of the ring, is unrelated to the Fermi surface topology and depends on the presence of the long-range Coulomb interaction. $\mathbf{Q}$ is defined as the momentum $\mathbf{q}$ where the maximum of $\mathrm{Re}\chi_{ch}(\mathbf{q}, \omega = 0)$ is located. To quantify the doping dependence, for instance, Fig. 4(a) shows that while the doping almost doubles between C and D, $|\mathbf{Q}|$ increases by $\sim 50\%$ in the axial direction and by $\sim 35\%$ in the diagonal direction. In addition, as can be seen also in Figs. 4(b)–4(e) and Figs. 6(c)–6(f), the intensity

of the ring decreases and the ring widens with increasing doping away from the RP instability line. It is important to mention that the ring-shaped structures are not exactly rings in the mathematical sense. Although within the thickness of the RP instability line the static charge susceptibility diverges for all wave vectors along the ring, which motivates the name RP, in the translation-invariant phase the intensity of the ring has a modulation with a maximum at the axial (diagonal) direction for h-cuprates (e-cuprates). In Figs. 4(b)–4(e) [Figs. 6(c)–6(f)] we can see well-defined rings; however they have a very weak intensity modulation, indiscernible in the intensity maps but noticeable in the cuts in Fig. 4(a) [Fig. 6(b)], with maximum at the axial (diagonal) direction.

$|\mathbf{Q}|$ depends also on the strength of the long-range Coulomb interaction V_c. $|\mathbf{Q}|$ increases with increasing V_c which can be seen after comparing Figs. 4(b)–4(e) and Figs. 6(c)–6(f), for $V_c = 1$, with Figs. 7(b)–7(d) for the realistic value of $V_c = 20$. In addition, the anisotropy along the ring is more evident at low energy [Fig. 7(b) and Fig. 8(b)] for realistic values of the long-range Coulomb interaction,

where, as in the experiment, the largest intensity is at the axial directions.

Our results capture several important details of the experiment. Dynamic ring-shaped charge modulations exist in the presence of the long-range Coulomb interaction in the translation-invariant phase. However, it is a prerequisite for the existence of rings that without long-range $V(\mathbf{q})$ the system shows PS.

[1] G. Ghiringhelli, M. Le Tacon, M. Minola, S. Blanco-Canosa, C. Mazzoli, N. B. Brookes, G. M. De Luca, A. Frano, D. G. Hawthorn, F. He, T. Loew, M. M. Sala, D. C. Peets, M. Salluzzo, E. Schierle, R. Sutarto, G. A. Sawatzky, E. Weschke, B. Keimer, and L. Braicovich, Long-range incommensurate charge fluctuations in (Y, Nd)Ba$_2$Cu$_3$O$_{6+x}$, Science **337**, 821 (2012).

[2] J. Chang, E. Blackburn, A. T. Holmes, N. B. Christensen, J. Larsen, J. Mesot, R. Liang, D. A. Bonn, W. N. Hardy, A. Watenphul, M. v. Zimmermann, E. M. Forgan, and S. M. Hayden, Direct observation of competition between superconductivity and charge density wave order in YBa$_2$Cu$_3$O$_{6.67}$, Nat. Phys. **8**, 871 (2012).

[3] A. J. Achkar, R. Sutarto, X. Mao, F. He, A. Frano, S. Blanco-Canosa, M. Le Tacon, G. Ghiringhelli, L. Braicovich, M. Minola, M. Moretti Sala, C. Mazzoli, R. Liang, D. A. Bonn, W. N. Hardy, B. Keimer, G. A. Sawatzky, and D. G. Hawthorn, Distinct Charge Orders in the Planes and Chains of Ortho-III-Ordered YBa$_2$Cu$_3$O$_{6+\delta}$ Superconductors Identified by Resonant Elastic X-Ray Scattering, Phys. Rev. Lett. **109**, 167001 (2012).

[4] E. Blackburn, J. Chang, M. Hücker, A. T. Holmes, N. B. Christensen, R. Liang, D. A. Bonn, W. N. Hardy, U. Rütt, O. Gutowski, M. v. Zimmermann, E. M. Forgan, and S. M. Hayden, X-Ray Diffraction Observations of a Charge-Density-Wave Order in Superconducting Ortho-II YBa$_2$Cu$_3$O$_{6.54}$ Single Crystals in Zero Magnetic Field, Phys. Rev. Lett. **110**, 137004 (2013).

[5] S. Blanco-Canosa, A. Frano, E. Schierle, J. Porras, T. Loew, M. Minola, M. Bluschke, E. Weschke, B. Keimer, and M. Le Tacon, Resonant x-ray scattering study of charge-density-wave correlations in YBa$_2$Cu$_3$O$_{6+x}$, Phys. Rev. B **90**, 054513 (2014).

[6] R. Comin, A. Frano, M. M. Yee, Y. Yoshida, H. Eisaki, E. Schierle, E. Weschke, R. Sutarto, F. He, A. Soumyanarayanan, Y. He, M. Le Tacon, I. S. Elfimov, J. E. Hoffman, G. A.

Sawatzky, B. Keimer, and A. Damascelli, Charge order driven by Fermi-arc instability in Bi$_2$Sr$_{2−x}$La$_x$CuO$_{6+\delta}$, Science **343**, 390 (2014).

[7] R. Comin, R. Sutarto, F. He, E. H. da Silva Neto, L. Chauviere, A. Fraño, R. Liang, W. N. Hardy, D. A. Bonn, Y. Yoshida, H. Eisaki, A. J. Achkar, D. G. Hawthorn, B. Keimer, G. A. Sawatzky, and A. Damascelli, Symmetry of charge order in cuprates, Nat. Mater. **14**, 796 (2015).

[8] E. H. da Silva Neto, P. Aynajian, A. Frano, R. Comin, E. Schierle, E. Weschke, A. Gyenis, J. Wen, J. Schneeloch, Z. Xu, S. Ono, G. Gu, M. Le Tacon, and A. Yazdani, Ubiquitous interplay between charge ordering and high-temperature superconductivity in cuprates, Science **343**, 393 (2014).

[9] W. Tabis, Y. Li, M. L. Tacon, L. Braicovich, A. Kreyssig, M. Minola, G. Dellea, E. Weschke, M. J. Veit, M. Ramazanoglu, A. I. Goldman, T. Schmitt, G. Ghiringhelli, N. Barisic, M. K. Chan, C. J. Dorow, G. Yu, X. Zhao, B. Keimer, and M. Greven, Charge order and its connection with Fermi-liquid charge transport in a pristine high-T_c cuprate, Nat. Commun. **5**, 5875 (2014).

[10] S. Gerber, H. Jang, H. Nojiri, S. Matsuzawa, H. Yasumura, D. A. Bonn, R. Liang, W. N. Hardy, Z. Islam, A. Mehta, S. Song, M. Sikorski, D. Stefanescu, Y. Feng, S. A. Kivelson, T. P. Devereaux, Z.-X. Shen, C.-C. Kao, W.-S. Lee, D. Zhu *et al.*, Three-dimensional charge density wave order in YBa$_2$Cu$_3$O$_{6.67}$ at high magnetic fields, Science **350**, 949 (2015).

[11] W. Tabis, B. Yu, I. Bialo, M. Bluschke, T. Kolodziej, A. Kozlowski, E. Blackburn, K. Sen, E. M. Forgan, M. v. Zimmermann, Y. Tang, E. Weschke, B. Vignolle, M. Hepting, H. Gretarsson, R. Sutarto, F. He, M. Le Tacon, N. Barišić, G. Yu *et al.*, Synchrotron x-ray scattering study of charge-density-wave order in HgBa$_2$CuO$_{4+\delta}$, Phys. Rev. B **96**, 134510 (2017).

[12] E. H. da Silva Neto, R. Comin, F. He, R. Sutarto, Y. Jiang, R. L. Greene, G. A. Sawatzky, and A. Damascelli, Charge ordering in the electron-doped superconductor Nd$_{2−x}$Ce$_x$CuO$_4$, Science **347**, 282 (2015).

[13] E. H. da Silva Neto, B. Yu, M. Minola, R. Sutarto, E. Schierle, F. Boschini, M. Zonno, M. Bluschke, J. Higgins, Y. Li, G. Yu, E. Weschke, F. He, M. Le Tacon, R. L. Greene, M. Greven, G. A. Sawatzky, B. Keimer, and A. Damascelli, Doping-dependent charge order correlations in electron-doped cuprates, Sci. Adv. **2**, e1600782 (2016).

[14] E. H. da Silva Neto, M. Minola, B. Yu, W. Tabis, M. Bluschke, D. Unruh, H. Suzuki, Y. Li, G. Yu, D. Betto, K. Kummer, F. Yakhou, N. B. Brookes, M. Le Tacon, M. Greven, B. Keimer, and A. Damascelli, Coupling between dynamic magnetic and charge-order correlations in the cuprate superconductor $Nd_{2-x}Ce_xCuO_4$, Phys. Rev. B **98**, 161114(R) (2018).

[15] M. Bejas, A. Greco, and H. Yamase, Possible charge instabilities in two-dimensional doped Mott insulators, Phys. Rev. B **86**, 224509 (2012).

[16] A. Allais, J. Bauer, and S. Sachdev, Density wave instabilities in a correlated two-dimensional metal, Phys. Rev. B **90**, 155114 (2014).

[17] H. Meier, C. Pépin, M. Einenkel, and K. B. Efetov, Cascade of phase transitions in the vicinity of a quantum critical point, Phys. Rev. B **89**, 195115 (2014).

[18] Y. Wang and A. Chubukov, Charge-density-wave order with momentum $(2q, 0)$ and $(0, 2q)$ within the spin-fermion model: Continuous and discrete symmetry breaking, preemptive composite order, and relation to pseudogap in hole-doped cuprates, Phys. Rev. B **90**, 035149 (2014).

[19] W. A. Atkinson, A. P. Kampf, and S. Bulut, Charge order in the pseudogap phase of cuprate superconductors, New J. Phys. **17**, 013025 (2015).

[20] Y. Yamakawa and H. Kontani, Spin-Fluctuation-Driven Nematic Charge-Density Wave in Cuprate Superconductors: Impact of Aslamazov-Larkin Vertex Corrections, Phys. Rev. Lett. **114**, 257001 (2015).

[21] V. Mishra and M. R. Norman, Strong coupling critique of spin fluctuation driven charge order in underdoped cuprates, Phys. Rev. B **92**, 060507(R) (2015).

[22] R. Zeyher and A. Greco, Competition between spin-induced charge instabilities in underdoped cuprates, Phys. Rev. B **98**, 224504 (2018).

[23] S. Sachdev and R. La Placa, Bond Order in Two-Dimensional Metals with Antiferromagnetic Exchange Interactions, Phys. Rev. Lett. **111**, 027202 (2013).

[24] H. Yamase, M. Bejas, and A. Greco, Doping dependence of d-wave bond-charge excitations in electron-doped cuprates, Phys. Rev. B **99**, 014513 (2019).

[25] H. Yamase, Electronic nematic phase transition in the presence of anisotropy, Phys. Rev. B **91**, 195121 (2015).

[26] S. Banerjee, W. A. Atkinson, and A. P. Kampf, Emergent charge order from correlated electron-phonon physics in cuprates, Commun. Phys. **3**, 161 (2020).

[27] S. Caprara, C. Di Castro, G. Seibold, and M. Grilli, Dynamical charge density waves rule the phase diagram of cuprates, Phys. Rev. B **95**, 224511 (2017).

[28] S. Caprara, M. Grilli, C. Di Castro, and G. Seibold, Pseudogap and (an)isotropic scattering in the fluctuating charge-density wave phase of cuprates, J. Supercond. Novel Magn. **30**, 25 (2017).

[29] Y. Gannot, B. J. Ramshaw, and S. A. Kivelson, Fermi surface reconstruction by a charge density wave with finite correlation length, Phys. Rev. B **100**, 045128 (2019).

[30] L. Nie, L. E. H. Sierens, R. G. Melko, S. Sachdev, and S. A. Kivelson, Fluctuating orders and quenched randomness in the cuprates, Phys. Rev. B **92**, 174505 (2015).

[31] C. McMahon, A. J. Achkar, E. H. da Silva Neto, I. Djianto, J. Menard, F. He, R. Sutarto, R. Comin, R. Liang, D. A. Bonn, W. N. Hardy, A. Damascelli, and D. G. Hawthorn, Orbital symmetries of charge density wave order in $YBa_2Cu_3O_{6+x}$, Sci. Adv. **6**, eaay0345 (2020).

[32] F. Boschini, M. Minola, R. Sutarto, E. Schierle, M. Bluschke, S. Das, Y. Yang, M. Michiardi, Y. C. Shao, X. Feng, S. Ono, R. D. Zhong, J. A. Schneeloch, G. D. Gu, E. Weschke, F. He, Y. D. Chuang, B. Keimer, A. Damascelli, A. Frano *et al.*, Dynamic electron correlations with charge order wavelength along all directions in the copper oxide plane, Nat. Commun. **12**, 597 (2021).

[33] M. Kang, J. Pelliciari, A. Frano, N. Breznay, E. Schierle, E. Weschke, R. Sutarto, F. He, P. Shafer, E. Arenholz, M. Chen, K. Zhang, A. Ruiz, Z. Hao, S. Lewin, J. Analytis, Y. Krockenberger, H. Yamamoto, T. Das, and R. Comin, Evolution of charge order topology across a magnetic phase transition in cuprate superconductors, Nat. Phys. **15**, 335 (2019).

[34] D. C. Morse and T. C. Lubensky, Instabilities of the Fermi-liquid and staggered flux phases in the large-Nt-J model, Phys. Rev. B **43**, 10436 (1991).

[35] R. Zeyher and M. L. Kulić, Statics and dynamics of charge fluctuations in the t-J model, Phys. Rev. B **54**, 8985 (1996).

[36] A. Foussats and A. Greco, Large-N expansion based on the Hubbard operator path integral representation and its application to the t-J model. II. The case for finite J, Phys. Rev. B **70**, 205123 (2004).

[37] A. Greco and R. Zeyher, Collective excitations in unconventional charge-density wave systems, Phys. Rev. B **73**, 195126 (2006).

[38] Z. Wang, Strongly correlated Fermi liquid and the normal state of high-T_c superconductors, Int. J. Mod. Phys. B **06**, 603 (1992).

[39] I. Affleck and J. B. Marston, Large-N limit of the Heisenberg-Hubbard model: Implications for high-T_c superconductors, Phys. Rev. B **37**, 3774 (1988).

[40] G. Kotliar and J. Liu, Superexchange mechanism and d-wave superconductivity, Phys. Rev. B **38**, 5142 (1988).

[41] M. Grilli, R. Raimondi, C. Castellani, C. Di Castro, and G. Kotliar, Superconductivity, Phase Separation, and Charge-Transfer Instability in the $U = \infty$ Limit of the Three-Band Model of the CuO_2 Planes, Phys. Rev. Lett. **67**, 259 (1991).

[42] F. Becca, M. Tarquini, M. Grilli, and C. Di Castro, Charge-density waves and superconductivity as an alternative to phase separation in the infinite-U Hubbard-Holstein model, Phys. Rev. B **54**, 12443 (1996).

[43] C. Castellani, C. Di Castro, and M. Grilli, Singular Quasiparticle Scattering in the Proximity of Charge Instabilities, Phys. Rev. Lett. **75**, 4650 (1995).

[44] E. Cappelluti and R. Zeyher, Interplay between superconductivity and flux phase in the t-J model, Phys. Rev. B **59**, 6475 (1999).

[45] M. Bejas, H. Yamase, and A. Greco, Dual structure in the charge excitation spectrum of electron-doped cuprates, Phys. Rev. B **96**, 214513 (2017).

[46] S. Chakravarty, R. B. Laughlin, D. K. Morr, and C. Nayak, Hidden order in the cuprates, Phys. Rev. B **63**, 094503 (2001).

[47] G. B. Martins, J. C. Xavier, L. Arrachea, and E. Dagotto, Qualitative understanding of the sign of t' asymmetry in the extended t-J model and relevance for pairing properties, Phys. Rev. B **64**, 180513(R) (2001).

[48] T. Tohyama and S. Maekawa, Role of next-nearest-neighbor hopping in the t-t'-J model, Phys. Rev. B **49**, 3596 (1994).

[49] T. Tohyama, C. Gazza, C. T. Shih, Y. C. Chen, T. K. Lee, S. Maekawa, and E. Dagotto, Stripe stability in the extended t-J model on planes and four-leg ladders, Phys. Rev. B **59**, R11649 (1999).

[50] M. Bejas, A. Greco, and H. Yamase, Strong particle-hole asymmetry of charge instabilities in doped Mott insulators, New J. Phys. **16**, 123002 (2014).

[51] G. D. Mahan, *Many-Particle Physics*, 2nd ed. (Plenum Press, New York, 1990).

[52] F. C. Zhang and T. M. Rice, Effective Hamiltonian for the superconducting Cu oxides, Phys. Rev. B **37**, 3759 (1988).

[53] A. Macridin, M. Jarrell, and T. Maier, Phase separation in the Hubbard model using the dynamical cluster approximation, Phys. Rev. B **74**, 085104 (2006).

[54] A. Greco, H. Yamase, and M. Bejas, Close inspection of plasmon excitations in cuprate superconductors, Phys. Rev. B **102**, 024509 (2020).

[55] A. Nag, M. Zhu, M. Bejas, J. Li, H. C. Robarts, H. Yamase, A. N. Petsch, D. Song, H. Eisaki, A. C. Walters, M. García-Fernández, A. Greco, S. M. Hayden, and K.-J. Zhou, Detection of Acoustic Plasmons in Hole-Doped Lanthanum and Bismuth Cuprate Superconductors Using Resonant Inelastic X-Ray Scattering, Phys. Rev. Lett. **125**, 257002 (2020).

[56] M. Hepting, M. Bejas, A. Nag, H. Yamase, N. Coppola, D. Betto, C. Falter, M. Garcia-Fernandez, S. Agrestini, K.-J. Zhou, M. Minola, C. Sacco, L. Maritato, P. Orgiani, H. I. Wei, K. M. Shen, D. G. Schlom, A. Galdi, A. Greco, and B. Keimer, Gapped Collective Charge Excitations and Interlayer Hopping in Cuprate Superconductors, Phys. Rev. Lett. **129**, 047001 (2022).

[57] M. Hepting, L. Chaix, E. W. Huang, R. Fumagalli, Y. Y. Peng, B. Moritz, K. Kummer, N. B. Brookes, W. C. Lee, M. Hashimoto, T. Sarkar, J.-F. He, C. R. Rotundu, Y. S. Lee, R. L. Greene, L. Braicovich, G. Ghiringhelli, Z. X. Shen, T. P. Devereaux, and W. S. Lee, Three-dimensional collective charge excitations in electron-doped copper oxide superconductors, Nature (London) **563**, 374 (2018).

[58] J. Lin, J. Yuan, K. Jin, Z. Yin, G. Li, K.-J. Zhou, X. Lu, M. Dantz, T. Schmitt, H. Ding, H. Guo, M. P. M. Dean, and X. Liu, Doping evolution of the charge excitations and electron correlations in electron-doped superconducting $La_{2-x}Ce_xCuO_4$, npj Quantum Mater. **5**, 4 (2020).

[59] A. Singh, H. Y. Huang, C. Lane, J. H. Li, J. Okamoto, S. Komiya, R. S. Markiewicz, A. Bansil, T. K. Lee, A. Fujimori, C. T. Chen, and D. J. Huang, Acoustic plasmons and conducting carriers in hole-doped cuprate superconductors, Phys. Rev. B **105**, 235105 (2022).